



Numerical modeling of fault damage zones and their impact on EOR applications

Juliema Fronczak^{1,2}, Paul Ortega², Roberto Quevedo², Deane Roehl^{1,2}, Bruno Carvalho³,

¹ *Civil Engineering Department, PUC-Rio*

Rua Marquês de São Vicente, 225, 22453-900, Rio de Janeiro, Brazil

juliema.fronczak@aluno.puc-rio.br, droehl@puc-rio.br

² *Tecgraf Institute, PUC-Rio*

Rua Marquês de São Vicente, 225, 22453-900, Rio de Janeiro, Brazil

julief@tecgraf.puc-rio.br, paulortega @tecgraf.puc-rio.br, rquevedo@tecgraf.puc-rio.br,

deane@tecgraf.puc-rio.br

³ *Petrobras Research Center*

Av. Horácio Macedo, 950, 21941-915, Rio de Janeiro, Brazil

brcarvalho@petrobras.com.br

Abstract. Fault damage zones can have different impacts on reservoir fluid flow. For example, poorly consolidated or high porosity rocks are susceptible to deformation bands that act as barriers to fluid flow. On the other hand, hard and brittle rocks are prone to develop fracture networks, creating preferential flow paths. However, fault zones are usually considered impermeable in reservoir engineering applications, disregarding the impact of damage zones. In this study, we perform numerical simulations to evaluate the effect of damage zones composed of deformation bands or fractures in enhanced oil recovery applications. For this purpose, we first assess equivalent porosities and permeability representative of damage zones. Then, we consider such properties in a synthetic reservoir model and perform numerical simulations. The results show that the fault damage zone can significantly affect the dynamic reservoir behavior.

Keywords: damage zone, deformation band, discrete fracture network, oil recovery efficiency, Oda's method, two-phase flow simulation.

1 Introduction

Fault zones are heterogeneous and anisotropic lithological structures that can be divided into two main regions: the fault core and the damage zone [1,2]. Depending on the host rock and the level of deformation, the impact of fault zones on the reservoir dynamic can be relevant due to significant alterations in flow properties in these regions. In reservoir engineering applications, fault zones are usually considered impermeable barriers due to breccias, cataclasites, and gouges in the core, disregarding the presence of the damage zone. Such an assumption is acceptable when damage zone widths are very thin compared to the reservoir dimensions. However, damage zones can considerably affect production strategies in some situations, slowing or speeding up the flow processes. For example, deformation bands triggered in poorly consolidated rock layers by pore collapse or grain crushing tend to delay the flow processes[3].

On the other hand, fracture networks generally increase permeability, providing preferential paths for fluid flow [2]. Different empirical correlations have been proposed in the literature to characterize the flow behavior of those damage zones [4][5]. Most of them are used to obtain equivalent properties of the damage zone using fault attributes such as throw, length, and damage zone width, as well as representative parameters of deformation bands

or fractures [6] [7][8]. In this study, we evaluate the impact of damage zones in enhanced oil recovery applications using numerical simulations based on the finite volume method. For this purpose, we consider a reservoir model with a vertical fault between an oil production well and a water injection well. Equivalent properties corresponding to the fault damage zones are assessed, considering some correlations representative of deformation bands or fractures. Then, biphasic flow simulations are performed considering two sets of properties, one representing the intact rock and the other of the fault damage zone. The results show that damage zones composed of deformation bands and fractures slow down and speed up, respectively, oil production.

2 Model building

The workflow for model building involves the following steps: a) generation of a grid of cells representative of the reservoir and the fault, b) definition of equivalent properties representative of the damage zones composed of deformation bands or fractures, c) assigning properties to cells in both, the damage zone and the intact rock, and d) assigning initial and boundary conditions.

2.1 Model grid

The adopted geometry is based on a faulted reservoir model proposed in the literature [8]. A vertical elliptical surface defines the fault core with zero thickness, as shown in Figure 2a. Then, the damage zone around such a surface is assessed using the following data. A maximum fault throw (T) of 100 m occurs in the fault center. The top and bottom layers of the model are flat, with a total volume of 1000 x 1600 x 600 m³. Two grids were used in the study. The global grid was generated with cell sizes of 20 x 32 x 36 m (resulting in 23,040 cells), as shown in Figure 2b. Around the fault plane, a more refined mesh was employed to represent the damage zone, with cell sizes of 1 x 32 x 36 m, focusing on the yz-plane, as illustrated in Figure 2c. This refined grid was used to populate the damage zone with deformation bands or fractures, Figure 2c. The dimensions of the cells parallel to the fault (along the y and z axes) were not altered to avoid high computational costs.

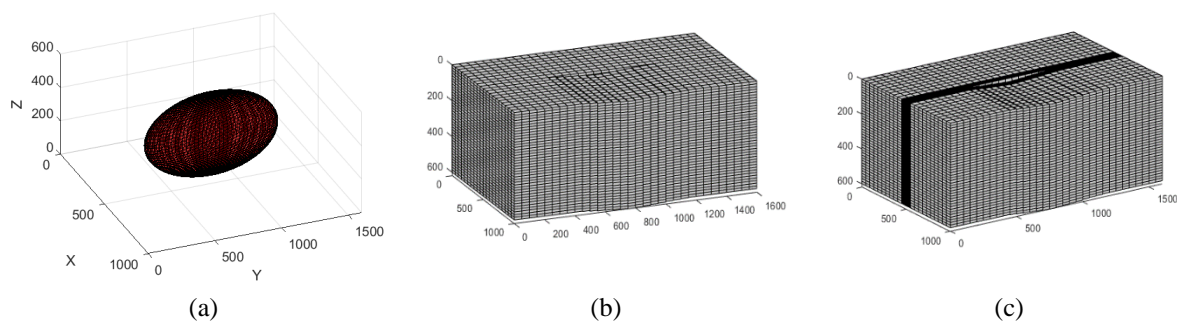


Figure 1. Synthetic structural model employed in this study. (a) elliptical surface of fault core (b) global grid with fault (c) refine mesh of grid around fault

2.2 Definition of cells containing damage zones and equivalent properties

As a first step, we define the throw distribution values in ranges from 100 m at the center of the fault to 0 m at its edges, Fig 2 (a). As a second step, we assess the damage zone width (W) considering a power law based on the fault throw [6], as defined by eq. (1)

$$W = \alpha T^b \quad (1)$$

Deformation bands and fracture networks are characterized according to their intensity obtained through the use of scanlines (P_{10}), a simple count along a linear sampling, and (P_{21}) measurements, a linear measurement along an aerial sampling (Stohler et al. [9]). The logarithmic decay function for any fault throw is proposed by Schueller et al. [6] and it is defined by eq. (2) :

$$Y = A + L \cdot \ln(X) \quad (2)$$

where A and L are constants, Y represents the number of deformation bands per meter, and X is the distance from the fault core. Based on the parameters A and L of the logarithmic decay function eq. (2) and the parameters a and b of the power law eq. (1) Stohler et al. [9] defined the logarithmic decay function for any throw value. The eq. (3) estimates the deformation band or fracture frequency distribution in damage zones for faults with any throws.

$$Y = [A + L(\ln(W) - \ln(aT^b)) + L \ln(X)] \quad (3)$$

In the present work, the logarithmic decay functions for any throw values to deformation bands or fractures are defined by eq. (4) and eq. (5), respectively.

$$Y = [30.731 - 5.838(\ln(W_{max}) - \ln(3.67T^{0.46})) + 5.838 \ln(X)] \quad (4)$$

$$Y = [4.68 - 0.66(\ln(W_{max}) - \ln(3.67T^{0.46})) + 0.66 \ln(X)] \quad (5)$$

where W_{max} is the value of the damage zone in the function of maximum throw of fault, eq. (1).

The constants for the logarithmic decay function of fractures are based on a database published by Maqbool et al. [10] and the constant for the deformation band is obtained from a database by Stohler et al. [9].

The next step is calculating the equivalent permeability to the damage zone with deformation bands and fractures. The harmonic mean method is used for the equivalent permeability of deformation bands, described in eq. (6), (7), (8)

$$k_{ef} = \frac{L_g}{\frac{l_{hr} + l_{db}}{k_{hr} + k_{db}}} \quad (6)$$

$$l_{db} = Y \cdot L_g \cdot d \quad (7)$$

$$l_{hr} = L_g - l_{db} \quad (8)$$

where k_{ef} is the effective permeability, L_g is the cell length, k_{hr} and k_{db} are the permeability of host rock and band deformation, respectively, d is the thickness of an individual deformation band. The accumulated thicknesses of the host rock and deformation bands over distance L are represented by l_{hr} and l_{db} , respectively. The effective porosity of each cell was calculated using arithmetic averaging, setting 0.25 for the undeformed cells and 0.05 for the cells containing deformation bands.

On the other hand, the equivalent permeability of the fracture network was estimated using the ODA permeability tensor component k_{ij} where the fracture tensor F_{ij} is estimated with empirical correlation [11], shown in eq. (9) and (10). Finally, the components of the permeability tensor are calculated by eq. (11):

$$F_{ij} = \frac{1}{V} \sum_{k=1}^N A_k T_k n_{ik} n_{jk} \quad (9)$$

$$T_k = \frac{e_k^3}{12} \quad (10)$$

$$k_{ij} = \lambda(F_{kk} \delta_{ij} - F_{ij}) \quad (11)$$

where V is the grid block volume, A is the area fracture, $n_{ik} n_{jk}$ are components of the unit normal vector of each fracture, T_k is the transmissivity of fractures calculated by eq. (10), e_k is the fracture aperture and δ_{ij} is the Kronecker delta. The porosity of the fractured system, ϕ_F , is defined by the product between the fracture intensity (P_{32}) and the fracture aperture (e) as

$$\phi_F = P_{32} \cdot e_k \quad (12)$$

2.3 Assignment of properties

The population of equivalent permeability and porosity in the reservoir assumes two regions: a) the damage zone and b) the intact or host rock. The permeability of the host rock is constant with horizontal permeabilities (k_x, k_y) of 1000md and a vertical permeability (k_z) of 100md. In the scenario of a damage zone with deformation bands, the equivalent permeability values are in the range from 2 md to 47 md, Fig. 2 (a), where the thickness (l_{db}) is 2mm and permeability (k_{db}) is 0.01md. These values are in the same order of magnitude as the results presented in the literature [2]. For the damage zone scenario with fractures, effective permeability is influenced by the area,

aperture, and orientation of the fractures. A fixed aperture of 0.0005m and an area of 24m² were considered for the fractures in the damage zone, having random trend and plunge angles as orientation. Fig. 2 (b) shows equivalent permeability values ranging from 7md to 0.235d.

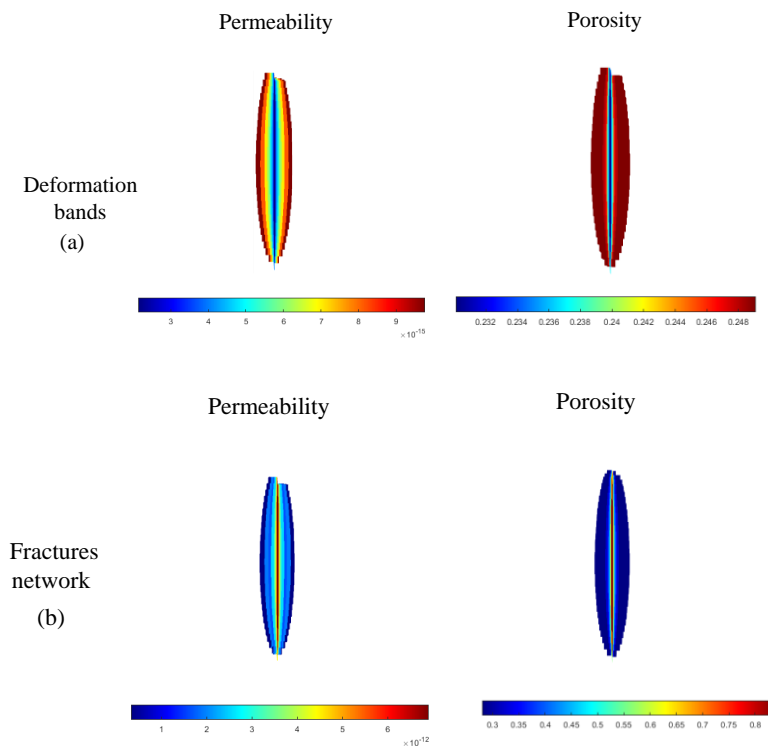


Figure 2. Equivalent permeability and porosity of the damage zone for a) deformation bands and b) fractures network.

2.4 Assignment of initial and boundary conditions

The top and bottom boundaries are defined as impermeable, and the lateral sides are Dirichlet. The porosity and permeability values for each cell in the damage zone are assigned according to Fig. 2. The MRST [12] application was used to simulate the oil-water system. An initial oil saturation of 0.8 was adopted in the entire model. A vertical water injection well and a vertical oil production well cross the whole reservoir. All simulations run for 11 years, considering a maximum time step of 50 days. The parameters and operation conditions used in the simulation are detailed in Table 1. The relative permeability curve employed is shown in Fig. 3.

Table 1. Flow Simulation Dynamic Properties

Parameters	Values
Rock compressibility (/bar)	0.000056
Oil density (kg/m ³)	883
Water density (kg/m ³)	1038
Water formation factor (cp)	0.42
Oil viscosity (cp)	1.04-1.32
Oil formation factor	1.22-1.26
Model top (m)	1800
Well injection rate (SM ³ /day)	55000
Production rate (SM ³ /day)	50000
Injection bottom-hole pressure (bar)	390
Producer bottom-hole pressure (bar)	227

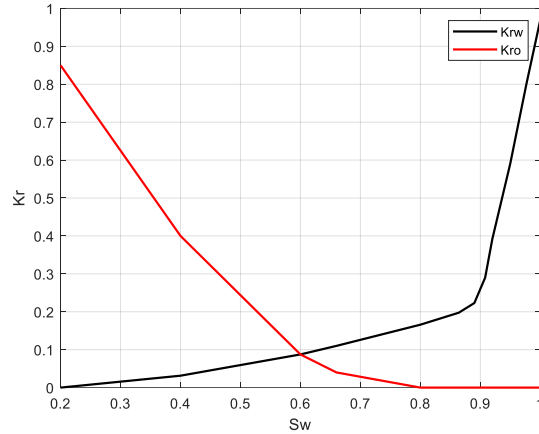


Figure 3. Permeability curves adopted in the flow simulations. K_r is the relative permeability, K_{ro} oil relative permeability, K_{rw} water relative permeability, and S_w water saturation.

3 Numerical Simulations and Results

Figure 4 shows the simulation model results for the reservoir's oil saturation distribution after 2 and 11 years of water injection for the three scenarios: a) no damage zone, b) damage zone with deformation bands, and c) damage zone with fracture network. The difference between the scenarios becomes even more pronounced. In the scenarios without damage zone and with fracture, water has already swept a large part of the reservoir, while in the scenario with deformation bands, there are still areas with high oil saturation. In the latter scenario, the waterfront advances more slowly and irregularly, resulting in a lower volume of oil recovered.

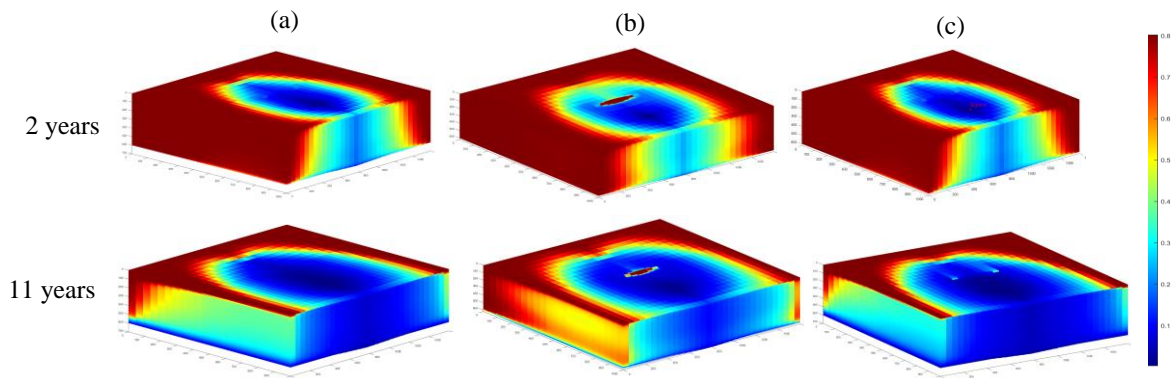


Figure 4. Oil saturation in the reservoir for 2 and 11 years of water injection in a) no damage zone, b) damage zone with deformation bands, and c) damage zone with fractures network.

The oil saturation distribution in a cross-section located at the fault center comparing the three models after 2 and 11 years of water injection is shown in Fig. 5. After two years, the waterfront in the model without damage zone advances homogeneously and symmetrically, in contrast to the scenario with fractures, where the advance is faster and directed along the fracture. In the scenario with deformation bands, the water advance is slower and more irregular. After 11 years, the difference between the scenarios becomes more pronounced. Water has already swept a large part of the reservoir in the scenarios without damage zone and with fractures. In contrast, there are still areas with high oil saturation in the scenario with deformation bands.

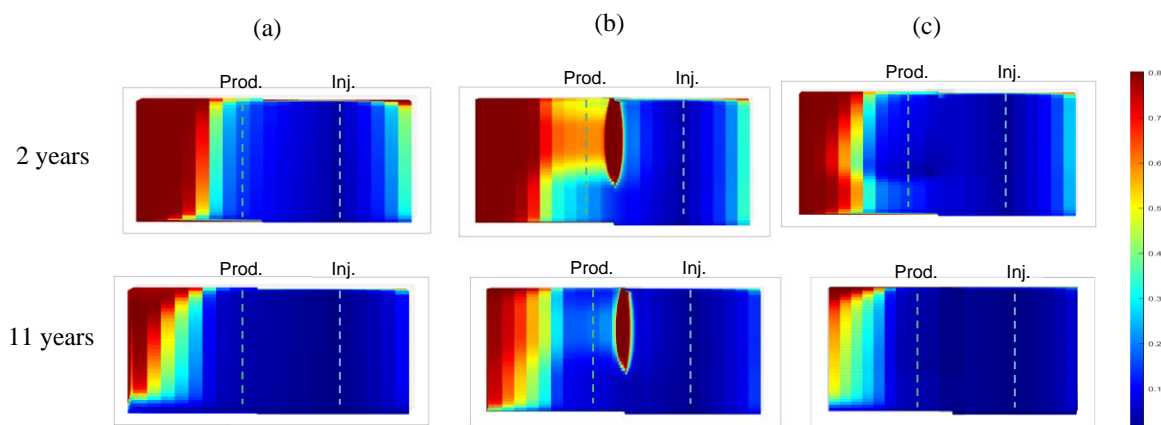


Figure 5. Oil saturation in cross-section modeling for 2 and 11 years in scenarios: a) no damage zone, b) damage zone with deformation bands, and c) damage zone with fractures network.

Considering the three scenarios, the water breakthrough in the production well over time is shown in Fig. 6 (a). In the scenario without a damage zone, water saturation increases rapidly in the first 392 days, reaching about 60% in the first few days. In the scenario with fractures, water saturation also increases quickly at the simulation's beginning, with a water breakthrough time of 196 days, reaching about 80% saturation in 1000 days. In the scenario with deformation bands, the increase in water saturation is slower and more gradual compared to the other two scenarios. Water breakthrough starts at 784 days. Water saturation reaches about 60% in 2000 days and continues to increase slowly throughout the simulation without reaching values as high as in the other scenarios. The results in Fig. 6 (b) show the values of the oil recovery coefficient. The differences in the recovery value for the three scenarios are small: 0.67 for the scenario without deformation bands and fractures, 0.72 with deformation bands, and 0.745 with fractures.

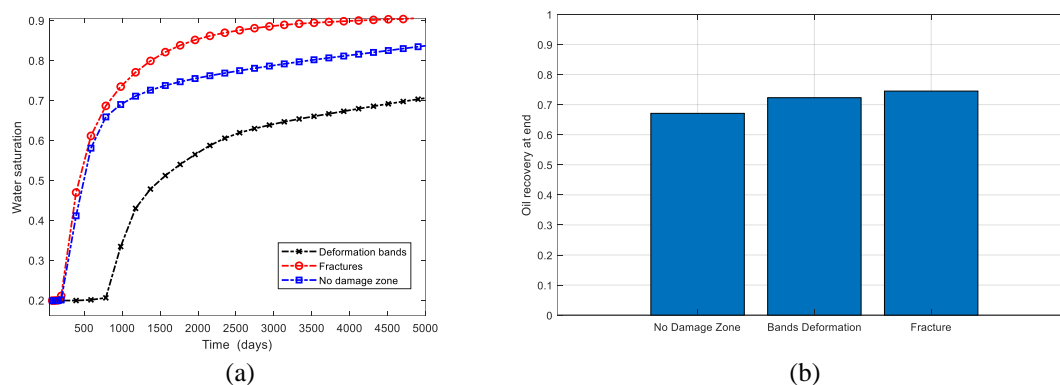


Figure 6. Reservoir responses of models (a) Time to water breakthrough for the three scenarios, (b) oil recovery at the end of the simulation

4 Conclusions

The numerical modeling simulation proposed in this study to evaluate the impact of damage zones, including deformation bands and fracture networks, shows that the presence of these structures affects the fluid flow, water breakthrough, and oil recovery process. Deformation bands, with their low permeability, act as barriers to water flow, delaying the advance of the waterfront and reducing oil displacement. Consequently, water breakthrough is retarded, and oil recovery is slightly higher compared to the scenario without a damage zone. On the other hand, fractures increase the permeability, facilitating water flow and accelerating the advance of the waterfront. The results presented in this work demonstrate the importance of incorporating structures such as deformation bands and fractures to evaluate oil recovery processes.

Acknowledgements. This research was carried out in association with the ongoing R&D project registered as ANP n° 21475-9, “GeoBanD 2 – Geomodelagem de zona de dano em falhas geológicas” (PUC-Rio/CENPES/ANP), sponsored by Petrobras. The authors also gratefully acknowledge the support from Carlos Chagas Filho Foundation for Supporting Research in the State of Rio de Janeiro (FAPERJ) Grant E-26/211.766/2021-0, Brazilian National Council for Scientific and Technological Development (CNPq) Grants 141617/2020-9, 420074/2021, and 407388/2022-2, and Tecgraf/PUC-Rio Institute. This study was financed in part by the 141201/2023-1.

Authorship statement. The authors hereby confirm that they are the sole liable persons responsible for the authorship of this work, and that all material that has been herein included as part of the present paper is either the property (and authorship) of the authors or has the permission of the owners to be included here.

References

- [1] H. Fossen and A. Rotevatn, “Fault linkage and relay structures in extensional settings-A review,” *Earth-Science Rev.*, vol. 154, pp. 14–28, 2016, doi: 10.1016/j.earscirev.2015.11.014.
- [2] A. Torabi, T. S. S. Ellingsen, M. U. Johannessen, B. Alaei, A. Rotevatn, and D. Chiarella, “Fault zone architecture and its scaling laws: where does the damage zone start and stop?,” *Geol. Soc. London, Spec. Publ.*, vol. 496, no. 1, pp. 99–124, 2020, doi: 10.1144/SP496-2018-151.
- [3] R. Quevedo, T. J. de Andrade, L. Santos, B. R. B. M. Carvalho, and D. Roehl, “Assessment of fault damage zones in carbonate rocks based on numerical and sensitivity analyses,” *Tectonophysics*, vol. 864, no. September, p. 230023, 2023, doi: 10.1016/j.tecto.2023.230023.
- [4] A. Aydin, R. I. Borja, and P. Eichhubl, “Geological and mathematical framework for failure modes in granular rock,” *J. Struct. Geol.*, vol. 28, no. 1, pp. 83–98, 2006, doi: 10.1016/j.jsg.2005.07.008.
- [5] A. Rotevatn, S. J. Buckley, J. A. Howell, and H. Fossen, “Overlapping faults and their effect on fluid flow in different reservoir types: A LIDAR-based outcrop modeling and flow simulation study,” *Am. Assoc. Pet. Geol. Bull.*, vol. 93, no. 3, pp. 407–427, 2009, doi: 10.1306/09300807092.
- [6] S. Schueller, A. Braathen, H. Fossen, and J. Tveranger, “Spatial distribution of deformation bands in damage zones of extensional faults in porous sandstones: Statistical analysis of field data,” *J. Struct. Geol.*, vol. 52, no. 1, pp. 148–162, 2013, doi: 10.1016/j.jsg.2013.03.013.
- [7] R. E. B. Araujo *et al.*, “Basement control on fault formation and deformation band damage zone evolution in the Rio do Peixe Basin, Brazil,” *Tectonophysics*, vol. 745, no. August, pp. 117–131, 2018, doi: 10.1016/j.tecto.2018.08.011.
- [8] D. Qu and J. Tveranger, “Incorporation of deformation band fault damage zones in reservoir models,” *Am. Assoc. Pet. Geol. Bull.*, vol. 100, no. 03, pp. 423–443, Mar. 2016, doi: 10.1306/12111514166.
- [9] R. C. Stohler, F. C. C. Nogueira, C. L. Mello, and J. A. B. Souza, “3D numerical modelling and simulation of the impact of fault zones on fluid flow in sandstones of the Rio do Peixe Basin, NE Brazil,” *Pet. Geosci.*, vol. 28, no. 4, 2022, doi: 10.1144/petgeo2022-024.
- [10] A. ur R. Maqbool, A. R. Moustafa, H. Dowidar, and M. Yousef, “Architecture of fault damage zones of normal faults, Gebel Ataqa area, Gulf of Suez rift, Egypt,” *Mar. Pet. Geol.*, vol. 77, pp. 43–53, 2016, doi: 10.1016/j.marpetgeo.2016.04.012.
- [11] B. Dershowitz, P. LaPointe, T. Eiben, and L. Wei, “Integration of discrete feature network methods with conventional simulator approaches,” *SPE Reserv. Eval. Eng.*, vol. 3, no. 2, pp. 165–170, 2000, doi: 10.2118/62498-PA.
- [12] *Advanced Modeling with the MATLAB Reservoir Simulation Toolbox*. 2021. doi: 10.1017/9781009019781.